

be used by cells. Yet, because reliable information transmission is a fundamental function of cellular signaling networks, it is plausible that evolutionary pressures shaped the cellular machinery to maximize the reliable decoding of multivariate dynamic signals.

## REFERENCES AND NOTES

- M. D. Brennan, R. Cheong, A. Levchenko, *Science* **338**, 334–335 (2012).
- A. Rhee, R. Cheong, A. Levchenko, *Phys. Biol.* **9**, 045011 (2012).
- C. Waltermann, E. Klipp, *Biochim. Biophys. Acta* **1810**, 924–932 (2011).
- F. Tostevin, P. R. ten Wolde, *Phys. Rev. Lett.* **102**, 218101 (2009).
- W. H. de Ronde, F. Tostevin, P. R. ten Wolde, *Phys. Rev. E Stat. Nonlin. Soft Matter Phys.* **82**, 031914 (2010).
- W. H. de Ronde, F. Tostevin, P. R. Ten Wolde, *Phys. Rev. E Stat. Nonlin. Soft Matter Phys.* **86**, 021913 (2012).
- G. Tkacik, C. G. Callan Jr., W. Bialek, *Proc. Natl. Acad. Sci. U.S.A.* **105**, 12265–12270 (2008).
- A. M. Walczak, G. Tkačik, W. Bialek, *Phys. Rev. E Stat. Nonlin. Soft Matter Phys.* **81**, 041905 (2010).
- P. Mehta, S. Goyal, T. Long, B. L. Bassler, N. S. Wingreen, *Mol. Syst. Biol.* **5**, 325 (2009).
- R. C. Yu et al., *Nature* **456**, 755–761 (2008).
- M. Behar, A. Hoffmann, *Biophys. J.* **105**, 231–241 (2013).
- R. Cheong, A. Rhee, C. J. Wang, I. Nemenman, A. Levchenko, *Science* **334**, 354–358 (2011).
- S. Uda et al., *Science* **341**, 558–561 (2013).
- M. Voliotis, R. M. Perrett, C. McWilliams, C. A. McArdle, C. G. Bowsher, *Proc. Natl. Acad. Sci. U.S.A.* **111**, E326–E333 (2014).
- N. Hao, B. A. Budnik, J. Gunawardena, E. K. O'Shea, *Science* **339**, 460–464 (2013).
- A. Hoffmann, A. Levchenko, M. L. Scott, D. Baltimore, *Science* **298**, 1241–1245 (2002).
- S. D. M. Santos, P. J. Verwee, P. I. H. Bastiaens, *Nat. Cell Biol.* **9**, 324–330 (2007).
- J. E. Purvis, G. Lahav, *Cell* **152**, 945–956 (2013).
- T. M. Cover, J. A. Thomas, *Elements of Information Theory 2nd* (Wiley-Interscience, ed. 2, Hoboken, NJ 2006).
- R. E. C. Lee, S. R. Walker, K. Savery, D. A. Frank, S. Gaudet, *Mol. Cell* **53**, 867–879 (2014).
- C. Cohen-Saidon, A. A. Cohen, A. Sigal, Y. Liron, U. Alon, *Mol. Cell* **36**, 885–893 (2009).
- O. E. Sturm et al., *Sci. Signal.* **3**, ra90 (2010).
- T. Schreiber, *Phys. Rep.* **308**, 1–64 (1999).
- J. E. Toettcher, O. D. Weiner, W. A. Lim, *Cell* **155**, 1422–1434 (2013).
- G. von Dassow, E. Meir, E. M. Munro, G. M. Odell, *Nature* **406**, 188–192 (2000).
- N. Barkai, S. Leibler, *Nature* **387**, 913–917 (1997).

## ACKNOWLEDGMENTS

We are indebted to T. Kemp (Univ. of California–San Diego) for discussion of the random Gram matrix theory. Supported by the NIH grants P50-GM085764 (R.W., A.H., L.T.), R01-GM089976 (L.T.), and R01-GM071573 (A.H.).

## SUPPLEMENTARY MATERIALS

www.sciencemag.org/content/346/6215/1370/suppl/DC1  
Supplementary Text  
Figs. S1 to S25  
Tables S1 to S6  
References (27–38)

17 April 2014; accepted 12 November 2014  
10.1126/science.1254933

## ONCOGENE REGULATION

# An oncogenic super-enhancer formed through somatic mutation of a noncoding intergenic element

Marc R. Mansour,<sup>1,2</sup> Brian J. Abraham,<sup>3\*</sup> Lars Anders,<sup>3\*</sup> Alla Berezovskaya,<sup>1</sup> Alejandro Gutierrez,<sup>1,4</sup> Adam D. Durbin,<sup>1</sup> Julia Etchin,<sup>1</sup> Lee Lawton,<sup>3</sup> Stephen E. Sallan,<sup>1,4</sup> Lewis B. Silverman,<sup>1,4</sup> Mignon L. Loh,<sup>5</sup> Stephen P. Hunger,<sup>6</sup> Takaomi Sanda,<sup>7</sup> Richard A. Young,<sup>3,8†</sup> A. Thomas Look<sup>1,4†</sup>

In certain human cancers, the expression of critical oncogenes is driven from large regulatory elements, called super-enhancers, that recruit much of the cell's transcriptional apparatus and are defined by extensive acetylation of histone H3 lysine 27 (H3K27ac). In a subset of T-cell acute lymphoblastic leukemia (T-ALL) cases, we found that heterozygous somatic mutations are acquired that introduce binding motifs for the MYB transcription factor in a precise noncoding site, which creates a super-enhancer upstream of the *TALI* oncogene. MYB binds to this new site and recruits its H3K27 acetylase-binding partner CBP, as well as core components of a major leukemogenic transcriptional complex that contains RUNX1, GATA-3, and *TALI* itself. Additionally, most endogenous super-enhancers found in T-ALL cells are occupied by MYB and CBP, which suggests a general role for MYB in super-enhancer initiation. Thus, this study identifies a genetic mechanism responsible for the generation of oncogenic super-enhancers in malignant cells.

In cancer cells, monoallelic expression of oncogenes can occur through a variety of mechanisms, including chromosomal translocation, alterations in promoter methylation, parental imprinting, and intrachromosomal deletion (1–3). A quintessential example is *TALI*<sup>d</sup>, an ~80-kilobase (kb) deletion on chromosome 1p33 that is found in 25% of cases of human T cell acute lymphoblastic leukemia (T-ALL). The deletion results in overexpression of *TALI*, an oncogene coding for a basic helix-loop-helix transcription factor, by mediating fusion of *TALI* coding sequences to the regulatory elements of the ubiquitously expressed gene “*SCL*-interrupting locus” (*STIL*) (4–6). However, we previously reported that a substantial proportion of T-ALLs, includ-

ing the Jurkat T-ALL cell line, have monoallelic overexpression of *TALI* but lack either the *TALI*<sup>d</sup> abnormality or a chromosomal translocation of the *TALI* locus (7, 8).

We hypothesized that cis-acting genomic lesions affecting *TALI* regulatory sequences might account for monoallelic *TALI* activation. Chromatin immunoprecipitation (ChIP)-sequencing (ChIP-seq) analysis of Jurkat cells revealed aberrant histone H3 lysine 27 acetylation (H3K27ac), a mark of active transcription, starting upstream of the *TALI* transcriptional start site and extending across the first exons (Fig. 1A) (9, 10). Regions with such rich and broad H3K27ac marks have been termed super-enhancers (also stretch enhancers or locus control regions) and are com-

monly found at genes that determine cell identity in embryonic stem (ES) cells and in tumor cells at oncogenes critical for the malignant cell state (11–17). The super-enhancer encompassing *TALI* in Jurkat cells was aberrant, in that it was not present in fetal thymocytes, normal CD34+ hematopoietic stem and progenitor cells (HSPCs), or in other T-ALL cell lines, such as *TALI*<sup>d</sup>-positive RPMI-8402 cells and DND-41 T-ALL cells that lack *TALI* expression (Fig. 1A) (9). Of note, chromatin conformation capture experiments recently performed in Jurkat cells identified a looping interaction involving an enhancer site 8 kb upstream of the transcription start site (TSS), which coincides with the locations of both the aberrant super-enhancer and the positive autoregulatory binding sites for members of the *TALI* complex in this cell line (Fig. 1A, red arrow) (9, 18).

Sequencing of the genomic DNA region encompassing this site identified a heterozygous 12-base pair (bp) insertion (GTTAGGAAACGG) that aligned precisely with the *TALI*, GATA3, RUNX1, and HEB ChIP-seq peaks (Fig. 1B). Among eight additional *TALI*-positive T-ALL cell lines, MOLT-3 cells also harbored an abnormal heterozygous 2-bp insertion (GT) at the same site (Fig. 1B), whereas none of 10

<sup>1</sup>Department of Pediatric Oncology, Dana-Farber Cancer Institute, Harvard Medical School, Boston, MA 02215, USA.

<sup>2</sup>Department of Haematology, UCL Cancer Institute, University College London, London WC1E 6BT, UK.

<sup>3</sup>Whitehead Institute for Biomedical Research, Cambridge, MA 02142, USA. <sup>4</sup>Division of Pediatric Hematology-Oncology, Boston Children's Hospital, MA 02115, USA. <sup>5</sup>Department of Pediatrics, Benioff Children's Hospital, University of California San Francisco, CA 94143, USA. <sup>6</sup>Pediatric Hematology/Oncology/BMT, University of Colorado School of Medicine and Children's Hospital Colorado, Aurora, CO 80045, USA. <sup>7</sup>Cancer Science Institute of Singapore, National University of Singapore, and Department of Medicine, Yong Loo Lin School of Medicine, 117599, Singapore. <sup>8</sup>Department of Biology, Massachusetts Institute of Technology, Cambridge, MA 02142, USA.

\*These authors contributed equally and are listed in alphabetical order. †Corresponding author. E-mail: thomas\_look@dfci.harvard.edu (A.T.L.); young@wi.mit.edu (R.A.Y.)

TAL1-negative cell lines had a detectable genomic abnormality in this region (table S1). Among 146 unselected pediatric primary T-ALL samples collected at diagnosis, eight patients (5.5%) had heterozygous indels 2 to 18 bp in length that overlapped at the same clearly defined hotspot (indels at this site are referred to here as “mutation of the TAL1 enhancer,” MuTE) (Fig. 1B). We estimate that MuTE abnormalities account

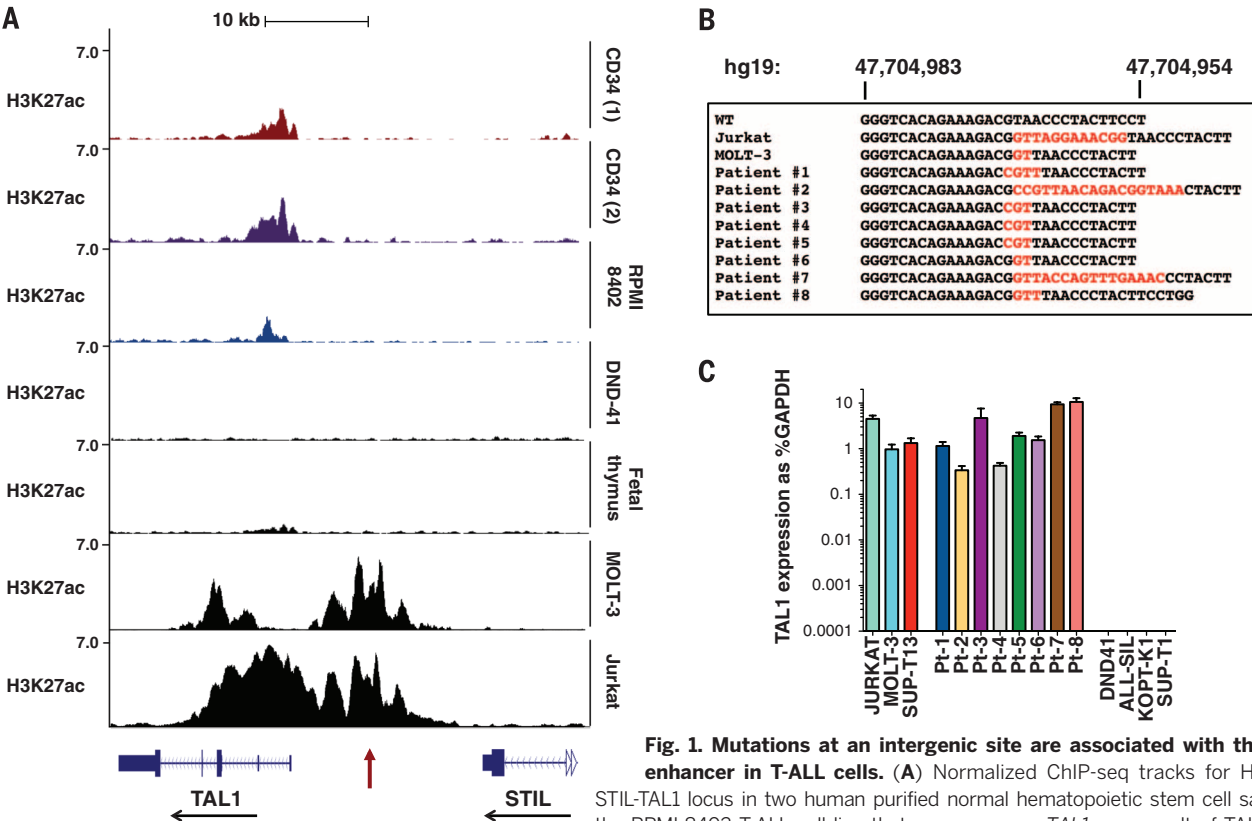


**Fig. 1. Mutations at an intergenic site are associated with the *TAL1* super-enhancer in T-ALL cells.** (A) Normalized ChIP-seq tracks for H3K27ac at the STIL-TAL1 locus in two human purified normal hematopoietic stem cell samples (CD34), the RPMI-8402 T-ALL cell line that overexpresses *TAL1* as a result of TAL1<sup>d</sup> (RPMI-8402

cells), DND-41 T-ALL cells that do not express *TAL1*, human fetal thymic tissue, and MOLT-3 and Jurkat cells that have mutations at a noncoding site 7.5 kb from the *TAL1* transcriptional start site (red arrow). Black arrows indicate the direction of transcription. ChIP-seq read densities (y axis) were normalized to reads per million reads sequenced in each sample. (B) Sequence alignments of the -7.5 kb site showing wild-type (WT) sequences in black and inserted sequences in red for Jurkat and MOLT-3 T-ALL cell lines and eight pediatric T-ALL patients. hg19, human genome build 19. (C) *TAL1* mRNA expression as determined by quantitative polymerase chain reaction (PCR) and expressed as percentage of glyceraldehyde-3-phosphate dehydrogenase (GAPDH). Error bars are  $\pm$  SEM from two independent experiments performed in triplicate.

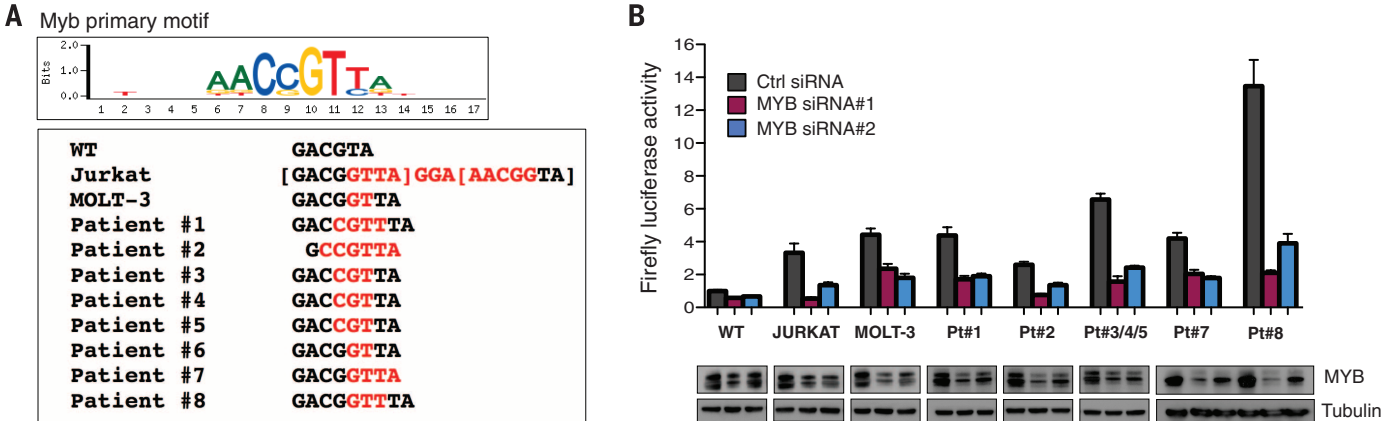


**Fig. 2. Mutations of the *TAL1* enhancer activate through recruitment of MYB.** (A) All *TAL1* enhancer mutations introduce de novo MYB binding sites as determined by UniPROBE (19). The MYB primary binding motif is shown above the mutation-derived MYB motifs, with inserted nucleotides shown in red. (B) A 400-bp fragment of the -7.5 kb *TAL1* enhancer containing the wild-type sequence or each of the mutant alleles was cloned upstream of luciferase and a minimal promoter. Constructs were delivered by the momentary creation

of small pores in cell membranes by applying an electrical pulse into Jurkat cells (electroporation), together with either control siRNA or two independent siRNAs targeting MYB. Firefly luciferase activity was measured at 24 hours, normalized to renilla luciferase to control for cell number and transfection efficiency, and expressed as a ratio relative to activity of the wild-type enhancer construct. Error bars are  $\pm$  SEM from two independent experiments performed in triplicate. Corresponding immunoblots for MYB and tubulin are shown below.

for about half of the cases with unexplained monoallelic overexpression of *TAL1* (7). Sequencing of DNA from remission bone marrow samples available from two mutation-positive patients showed wild-type sequences at this site, which indicated that the mutations were somatically acquired in the tumor cells. All eight MuTE-positive T-ALLs markedly overexpressed *TAL1* mRNA at levels comparable to those of the *TAL1*<sup>d</sup>-positive SUP-T13, and MuTE-positive Jurkat and MOLT-3 cells (Fig. 1C). Furthermore, MOLT-3 cells that share the same 2-bp insertion seen in patient 6 also had a super-enhancer at the *TAL1* locus (Fig. 1A).

To test our hypothesis that the aberrantly formed super-enhancer drives monoallelic *TAL1* expression, we analyzed the MuTE-positive samples for single-nucleotide polymorphisms in the 3' untranslated region (3' UTR) of the *TAL1* gene from genomic DNA. Jurkat cells and five of the patient samples were informative, and in each case, only one allele was detectable in the RNA sample, which indicated monoallelic expression of *TAL1* (fig. S1). We then used the UniPROBE

database to analyze whether the mutant sequences introduced new transcription factor binding sites (19). Note that all of the indels at this hotspot introduced de novo binding motifs for the MYB transcription factor, and two consecutive MYB binding motifs were generated by the 12-bp insertion in Jurkat cells (Fig. 2A and table S2).

To ascertain whether these mutations can activate gene expression, we cloned a 400-bp fragment containing either the wild-type allele or each of the *TAL1*-enhancer mutant alleles upstream of luciferase and tested the enhancer activity of this fragment in reporter assays. When we expressed these constructs in Jurkat cells, fragments containing each of the seven different mutations robustly increased reporter activity 3- to 14-fold as much as the wild-type fragment (Fig. 2B and fig. S2). Moreover, the activity of each of the mutant reporters was markedly reduced after MYB knockdown, which indicated that the enhancer activity imparted by the mutations was indeed mediated by MYB (Fig. 2B). When we performed these experiments in human

embryonic kidney 293T (HEK-293T) cells, the mutant reporters had no increased activity above that of the wild-type reporter (fig. S2), which suggested that transcription factors expressed in T-ALL, such as members of the TAL1 complex, are involved in activation of the mutant enhancer. We conclude that, in T-ALL primary samples and cell lines, indel mutations that introduce MYB binding sites at a hotspot 7.5 kb upstream from the TSS of *TAL1* generate a super-enhancer that drives monoallelic overexpression of this oncogene.

Our recent ChIP-seq studies of the TAL1 complex in T-ALL cells identified binding of transcription factors in the core TAL1 complex (TAL1, GATA3, RUNX1, E2A, and HEB) at the MYB enhancer, whereas knockdown of MYB generated a gene expression signature closely related to TAL1 knockdown (9, 10). We were technically unable to analyze MYB binding by ChIP-seq in our previous study, so at that time, we interpreted these results to indicate that MYB is a critical downstream hub of the TAL1 complex (10). However, in the current study we used newly available MYB-specific antibodies to generate high-resolution maps of genome-wide MYB binding in Jurkat cells. Analysis of the TAL1 enhancer indel mutation site in Jurkat cells showed precise alignment of MYB binding and binding of each member of the TAL1 complex (Fig. 3A). There was also an abundance of RNA polymerase II (Pol II) and Mediator (MED1), stretching over more than 20 kb, which indicated a large super-enhancer (table S3) (15). Notably, this site is also bound by MYB and TAL1 in MuTE-positive MOLT-3 cells (Fig. 3A) but not in RPMI-8402 and CCRF-CEM cells or a primary T-ALL sample, each of which overexpresses TAL1 driven by *TAL1*<sup>d</sup> (fig. S3). Nor were we able to detect binding of TAL1 at this site in HSPCs (fig. S3), which indicated that a small insertion creating a de novo MYB binding motif at this location is required for MYB binding and subsequent binding by other members of the TAL1 complex. Accordingly, knockdown of MYB resulted in depletion of *TAL1* expression in both Jurkat and MOLT-3 cells (fig. S4). Thus, MYB binding to the MuTE hotspot in a subset of *TAL1*-overexpressing T-ALLs results in the accumulation of an abundance of H3K27ac marks and aberrantly nucleates binding by other members of the TAL1 complex, leading to aberrant up-regulation of *TAL1* gene expression.

We next asked why the mutations we had identified in primary patient T-ALLs were clustered in a defined genomic location. A search for predicted transcription factor binding sites near the MuTE site identified the preferred binding sequences for RUNX1, GATA3, and ETS1, as well as E-box motifs characteristic of binding by TAL1/E-protein heterodimers (fig. S5). The absence of predicted MYB binding sites in the wild-type sequence suggests that the MuTE is critical for MYB binding and supports our hypothesis that MYB binding to its de novo motif is crucial to binding by members of the TAL1 complex at this hotspot. To explore this concept further, we extracted the raw ChIP-seq reads and determined the allelic frequency of

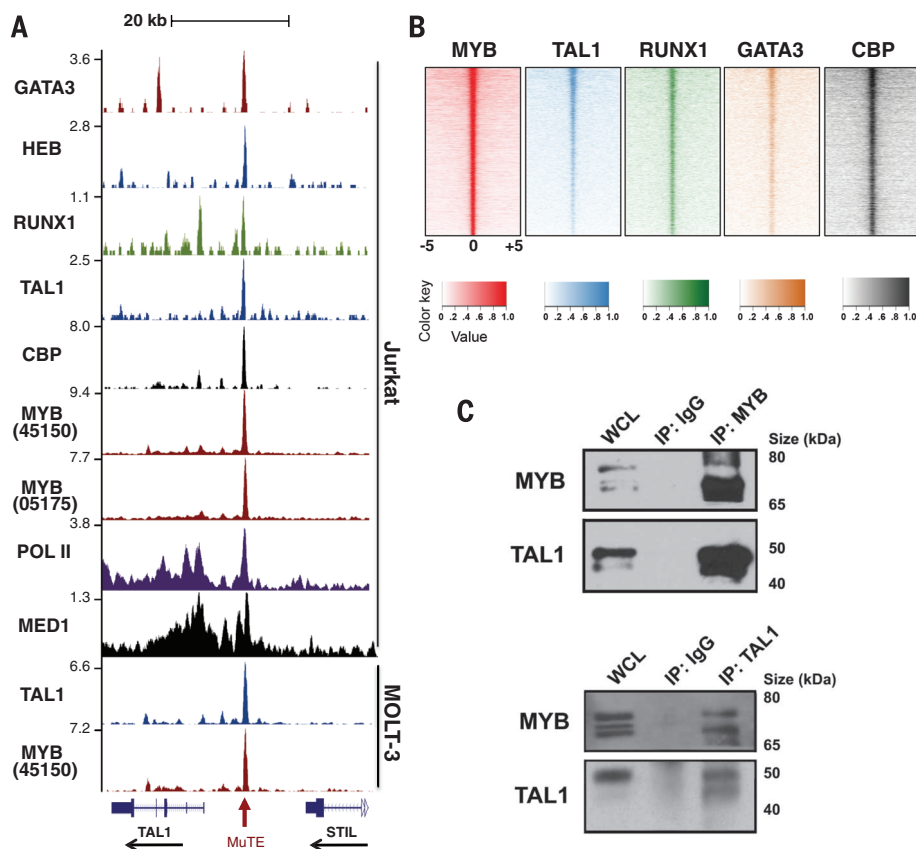


**Fig. 3. MYB binds the mutant *TAL1* enhancer site and is a member of the TAL1 complex.** (A) ChIP-seq tracks at the STIL-*TAL1* locus from Jurkat and MOLT-3 T-ALL cells for GATA3, HEB, RUNX1, TAL1, CBP, MYB (ab45150 antibody), MYB (05-175 antibody), RNA polymerase II (Pol II), and Mediator 1 (MED1). The mutation site at -7.5 kb is depicted with a red arrow. ChIP-seq read densities (y axis) were normalized to reads per million reads sequenced in each sample. (B) Heat maps showing genome-wide cococcupancy of MYB binding sites ( $\pm 5$  kb) with those from TAL1, RUNX1, GATA3, and CBP sites as determined by ChIP-seq. For each region (y axis), the read density centered at 0 indicates overlapping bound regions. (C) Co-IP and reciprocal Co-IP experiments performed from Jurkat lysates for MYB and TAL1. WCL, whole-cell lysate; IgG, isotype control immunoglobulin G antibody.



mutant to wild-type reads of bound DNA fragments at the mutation site. Note that, in MOLT-3 cells, both MYB and TAL1 bound predominantly to the mutant allele, with 67 of the 68 reads, and 37 of 38 reads, revealing the mutant sequence in the bound DNA. Likewise, in Jurkat cells, 404 of 419 reads, and 12 of 14 reads, contained the mutant sequence from MYB and TAL1 ChIP, which indicated that these transcription factors predominantly bind monoallelically to the mutant allele. Thus, our data indicate that indels producing MYB binding sites occur at a defined genomic location, probably because they must be in proximity to binding sites for other members of the TAL1 complex.

Given the well-established direct interaction between MYB and its potent transcriptional co-activator, CREB-binding protein (CBP) (20), we also analyzed ChIP-seq tracks for CBP in Jurkat cells and saw that CBP was also present at the *TAL1* enhancer indel mutation site (Fig. 3A). Because CBP promotes H3K27 acetylation and antagonizes Polycomb silencing (21), it seems likely that the initial event in the aberrant super-enhancer formation at this site is the recruitment of CBP by MYB, resulting in abundant H3K27 acetylation, which in turn opens the chromatin and permits binding by the other members of the TAL1 complex.

In a sense, the mutations forming MYB binding sites upstream of the *TAL1* gene in T-ALLs represent an “experiment of nature” that reveals the capacity of MYB binding to aberrantly nucleate a large super-enhancer that drives high levels of expression of a gene critical for the leukemic cell state. Thus, we interrogated the normal binding sites of MYB and observed highly concordant binding of MYB with members of the TAL1 complex throughout the genome (Fig. 3B), in that 80% of TAL1 binding sites were also cooccupied by MYB. We were also able to demonstrate a strong association of TAL1 and MYB proteins biochemically in reciprocal coimmunoprecipitation experiments (Fig. 3C). Next, we focused on the positive interconnected auto-regulatory loop that we had identified previously, whereby the core components of the TAL1 complex, TAL1, GATA3, and RUNX1, positively regulate their own enhancers (9). We found MYB bound with TAL1, GATA3, and RUNX1 at each of their respective enhancers, including one within the *MYB* gene itself (fig. S6). Notably, the TAL1 complex binding sites associated with all four of these genes also contained large super-enhancer domains, and all showed CBP-MYB cooccupancy. Furthermore, small interfering RNA (siRNA) knock-down of MYB was sufficient to deplete TAL1, GATA3, and RUNX1 (fig. S6). Thus, MYB is not

only a core component of the TAL1 complex but also a key factor involved in initiating the auto-regulatory positive-feedback circuitry (fig. S6).

To demonstrate definitively that MuTEs are responsible for TAL1 overexpression in a subset of T-ALL patients, we used clustered regularly interspaced short palindromic repeats (CRISPR)-associated (CRISPR-Cas9) technology to disrupt the MuTE site in Jurkat cells. Initially, we had difficulty expanding single-cell clones with deletion of the MuTE site, which suggested that deletion of the mutated enhancer site was diminishing TAL1 levels to a degree that impaired cell survival. Thus, we engineered Jurkat cells to express *TAL1* cDNA lacking the 3' UTR from a retroviral vector and performed all of our CRISPR-Cas9 experiments in these cells.

To directly target the enhancer mutation site in Jurkat cells, we first generated clones with a deletion of ~180 bp by targeting two guide RNAs to sites flanking either side of the enhancer mutation. Clones expanded from single cells harbored genomic deletions of 177 to 193 bp that involved the wild-type allele or mutant allele or both alleles (Fig. 4A and fig. S7). Deletion of the wild-type allele had no effect on endogenous *TAL1* mRNA levels, but deletion of the mutant allele completely abrogated endogenous *TAL1* expression, which indicated that the enhancer mutation

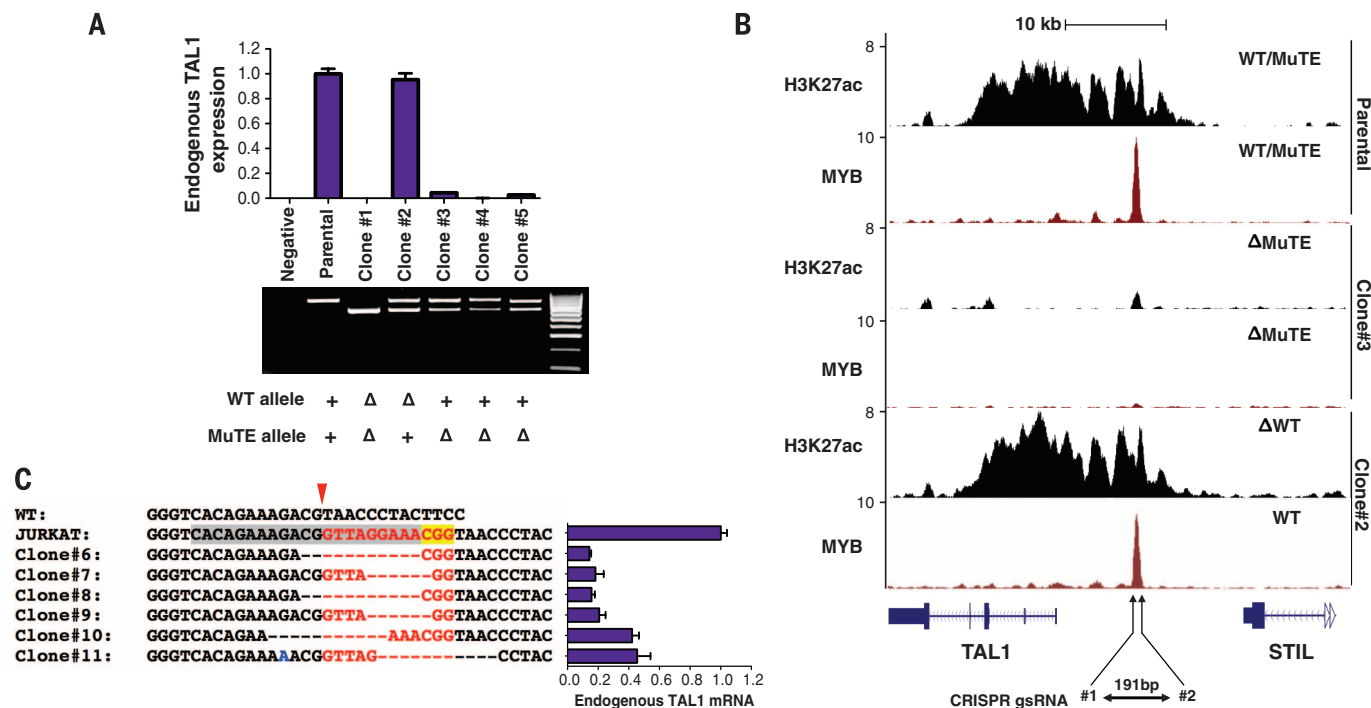


**Fig. 4. Targeted deletion of the *TAL1* enhancer mutation collapses the *TAL1* super-enhancer.** (A) Targeted deletion of 177 to 193 bp of the mutant, but not wild-type, allele in Jurkat cells abrogates expression of endogenous *TAL1*, as determined by quantitative reverse transcription PCR (qRT-PCR). Data are means  $\pm$  SD of two independent experiments performed in triplicate. Agarose gel of products from PCR amplification across the MuTE site for CRISPR-Cas9 Jurkat clones. All clones, including parental cells, express MSCV-*TAL1*. Hyperladder IV on right. Genotype for each clone is shown below: +, allele present; Δ, deleted allele. (B) ChIP-seq tracks for H3K27ac and

MYB at the *STIL*-*TAL1* locus from selected CRISPR-Cas9 clones. ChIP-seq read densities (y axis) were normalized to reads per million reads sequenced in each sample. (C) Sequence alignments of Jurkat clones targeted by CRISPR-Cas9 germline small RNA (gsRNA) number 3 [target sequence is highlighted in gray, protospacer adjacent motif (PAM) sequence in yellow], which targets the 12-bp insertion in Jurkat cells (red font) but not the wild-type allele. Endogenous *TAL1* expression as determined by qRT-PCR for respective clones is shown. Data are means  $\pm$  SD of two independent experiments performed in triplicate.

is responsible for *TALI* overexpression in these cells. Furthermore, ChIP-seq for H3K27ac showed complete collapse of the super-enhancer at the *TALI* locus when the deletion affected the allele with the enhancer mutation but was not affected when the deletion involved only the wild-type allele (Fig. 4B and figs. S8 and S9).

We also targeted a single guide RNA to specific sequences that form part of the 12-bp insertion in Jurkat cells, which permitted us to propagate single-cell clones with a spectrum of repair-induced indel mutations directly at the insertion site (Fig. 4C). In clones with deletion of 6 bp of the 12-bp enhancer insertion, encompassing one of the two inserted MYB binding sites, endogenous *TALI* expression levels decreased by ~60%, whereas clones with more extensive deletions had endogenous *TALI* expression levels decreased by ~85% (Fig. 4C). Thus, the MuTE is clearly responsible for *TALI* overexpression in Jurkat cells.

Our ChIP-seq results also show that MYB and CBP were bound together at 727 of the 818 (89%) super-enhancer regions that are present in Jurkat cells. When we performed short hairpin RNA-mediated knockdown for MYB, 221 of 818 (27%) super-enhancer-associated genes decreased significantly in expression (9, 17), which suggested that MYB has an active role in regulating their transcription. These results are consistent with the interpretation that MYB-CBP binding and the subsequent formation of abundant H3K27 acetylation marks may be broadly involved in the formation of super-enhancers in T-ALL. Thus, the role that we have shown for MYB binding in super-enhancer formation in a subset of T-ALLs with strategically placed somatic indel mutations in all likelihood provides insight into the general question of how super-enhancers are formed at the site of genes critical for the establishment of the T-ALL cell state. MYB is known to function as a master regulator of early and adult hematopoiesis and to undergo transcriptional down-regulation after lineage commitment and differentiation (22). An interesting area for future study will be to determine whether MYB acts in concert with CBP to regulate super-enhancer formation at genes critical for defining cell identity during normal hematopoietic cell differentiation (14, 16, 23, 24).

Our findings show that somatic mutation of noncoding intergenic elements can lead to binding of master transcription factors, such as MYB, which in turn aberrantly initiate super-enhancers that mediate overexpression of oncogenes. This raises the possibility that acquisition of such enhancer mutations may constitute a general mechanism of carcinogenesis used in other types of human cancers. Mechanisms of aberrant super-enhancer formation in malignancy have broad implications not only for molecular pathogenesis but also for clinical management. Drugs that target key components of the transcriptional machinery, such as BRD4 and CDK7 (12, 13, 17), have recently been shown to preferentially target tumor-specific super-enhancers, which provides a novel strategy to capitalize on these abnormalities for improved cancer therapy.

## REFERENCES AND NOTES

1. E. J. Walker et al., *Cancer Res.* **72**, 636–644 (2012).
2. A. Gimelbrant, J. N. Hutchinson, B. R. Thompson, A. Chess, *Science* **318**, 1136–1140 (2007).
3. R. L. Jirtle, *Exp. Cell Res.* **248**, 18–24 (1999).
4. T. M. Breit et al., *J. Exp. Med.* **177**, 965–977 (1993).
5. L. Brown et al., *EMBO J.* **9**, 3343–3351 (1990).
6. P. D. Aplan et al., *Science* **250**, 1426–1429 (1990).
7. A. A. Ferrando et al., *Blood* **103**, 1909–1911 (2004).
8. K. Leroy-Viard, M. A. Vinit, N. Lecoq, D. Mathieu-Mahul, P. H. Roméo, *Blood* **84**, 3819–3827 (1994).
9. T. Sanda et al., *Cancer Cell* **22**, 209–221 (2012).
10. M. R. Mansour et al., *J. Exp. Med.* **210**, 1545–1557 (2013).
11. R. Siersbæk et al., *Cell Rep.* **7**, 1443–1455 (2014).
12. J. Lovén et al., *Cell* **153**, 320–334 (2013).
13. P. Filippakopoulos et al., *Nature* **468**, 1067–1073 (2010).
14. S. C. Parker et al., *Proc. Natl. Acad. Sci. U.S.A.* **110**, 17921–17926 (2013).
15. D. Hnisz et al., *Cell* **155**, 934–947 (2013).
16. W. A. Whyte et al., *Cell* **153**, 307–319 (2013).
17. N. Kwiatkowski et al., *Nature* **511**, 616–620 (2014).
18. Y. Zhou et al., *Blood* **122**, 4199–4209 (2013).
19. D. E. Newburger, M. L. Bulyk, *Nucleic Acids Res.* **37** (Database), D77–D82 (2009).
20. P. Dai et al., *Genes Dev.* **10**, 528–540 (1996).
21. F. Tie et al., *Development* **141**, 1129–1139 (2014).
22. C. Schulz et al., *Science* **336**, 86–90 (2012).
23. A. Rada-Iglesias et al., *Nature* **470**, 279–283 (2011).
24. M. P. Creighton et al., *Proc. Natl. Acad. Sci. U.S.A.* **107**, 21931–21936 (2010).

## ACKNOWLEDGMENTS

We thank J. Gilbert for helpful editorial comments on the manuscript, J. Reddy for sharing data, and F. Alt and F. Meng for helpful advice on the design of the CRISPR experiments. We would

like to dedicate this paper to the memory of Michael Fayngersh. We gratefully acknowledge the children with T-ALL and their families for the samples analyzed in these studies. M.R.M. was supported by the Claudia Adams Barr Innovative Basic Science Research Program, the Kay Kendall Leukaemia Trust, and a Bennett Fellowship from Leukaemia and Lymphoma Research, UK. A.G. is a Research Fellow of the Gabrielle's Angel Foundation for Cancer Research, a Clinical Investigator of the Damon Runyon Cancer Research Foundation, and is supported by grants National Cancer Institute, NIH, CA167124, Department of Defense, CA120215 and an award from the William Lawrence and Blanche Hughes Foundation. T.S. is supported by a grant from the National Research Foundation (NRF), Prime Minister's Office, Singapore under its NRF Fellowship Program (award no. NRF-NRFF2013-02). This work was funded by NIH grants R01CA176746-01 and 5P01CA109901-08 (A.T.L.), and 5P01CA68484 (S.E.S. and A.T.L.). Children's Oncology Group cell banking and sample distribution were supported by grants CA98543, CA114766, CA98413, CA30969, and CA29139 from the NIH. S.P.H. is the Ergen Family Chair in Pediatric Cancer. R.A.Y. is a founder and member of the Board of Directors of Syros Pharmaceuticals, a company developing therapies that target gene regulatory elements including super-enhancers.

## SUPPLEMENTARY MATERIALS

www.sciencemag.org/content/346/6215/1373/suppl/DC1  
Materials and Methods

Figs. S1 to S9  
Tables S1 to S3  
References (25–44)

22 July 2014; accepted 4 November 2014  
Published online 13 November 2014;  
10.1126/science.1259037

## ELECTRON MICROSCOPY

# Ultrastable gold substrates for electron cryomicroscopy

Christopher J. Russo and Lori A. Passmore\*

Despite recent advances, the structures of many proteins cannot be determined by electron cryomicroscopy because the individual proteins move during irradiation. This blurs the images so that they cannot be aligned with each other to calculate a three-dimensional density. Much of this movement stems from instabilities in the carbon substrates used to support frozen samples in the microscope. Here we demonstrate a gold specimen support that nearly eliminates substrate motion during irradiation. This increases the subnanometer image contrast such that  $\alpha$  helices of individual proteins are resolved. With this improvement, we determine the structure of apoferritin, a smooth octahedral shell of  $\alpha$ -helical subunits that is particularly difficult to solve by electron microscopy. This advance in substrate design will enable the solution of currently intractable protein structures.

Recent developments in electron cryomicroscopy (cryo-EM) have allowed structure determination to near-atomic resolution for some macromolecular complexes (1–3). Still, many small and challenging structures cannot be determined by current cryo-EM methods to the resolutions required for accurate modeling of atom positions. This is because electron micrograph quality still falls short of the physical limits imposed by radiation damage to the macromolecules (4–6). Reduced image quality likely

has two primary origins: inefficient detection of imaging electrons (6, 7) and motion and blurring of the particles during irradiation (6, 8–11). Recent developments in electron detectors have addressed the first constraint (12, 13) and have enabled the development of motion correction algorithms to ameliorate the effects of the second (14–16). Direct electron detectors can acquire images using fractions of the electron dose previously required, thus allowing the measurement of single-molecule positions in time. This allows accurate tracking of large ensembles of particles and offers a way to determine the physical origins of radiation-induced particle movement (14–17).

Medical Research Council (MRC) Laboratory of Molecular Biology, Francis Crick Avenue, Cambridge CB2 0QH, UK.  
\*Corresponding author. E-mail: passmore@mrc-lmb.cam.ac.uk



## An oncogenic super-enhancer formed through somatic mutation of a noncoding intergenic element

Marc R. Mansour *et al.*  
*Science* **346**, 1373 (2014);  
DOI: 10.1126/science.1259037

*This copy is for your personal, non-commercial use only.*

If you wish to distribute this article to others, you can order high-quality copies for your colleagues, clients, or customers by [clicking here](#).

Permission to republish or repurpose articles or portions of articles can be obtained by following the guidelines [here](#).

**The following resources related to this article are available online at *www.sciencemag.org* (this information is current as of December 11, 2014 ):**

**Updated information and services**, including high-resolution figures, can be found in the online version of this article at:

<http://www.sciencemag.org/content/346/6215/1373.full.html>

**Supporting Online Material** can be found at:

<http://www.sciencemag.org/content/suppl/2014/11/12/science.1259037.DC1.html>

A list of selected additional articles on the Science Web sites **related to this article** can be found at:

<http://www.sciencemag.org/content/346/6215/1373.full.html#related>

This article **cites 44 articles**, 23 of which can be accessed free:

<http://www.sciencemag.org/content/346/6215/1373.full.html#ref-list-1>

This article appears in the following **subject collections**:

Medicine, Diseases

<http://www.sciencemag.org/cgi/collection/medicine>